Power-law behavior of transcriptional bursting regulated by enhancer–promoter communication

Zihao Wang, Zhenquan Zhang, Songhao Luo, et al.

Genome Res. 2024 34: 106-118 originally published online January 3, 2024
Access the most recent version at doi:10.1101/gr.278631.123

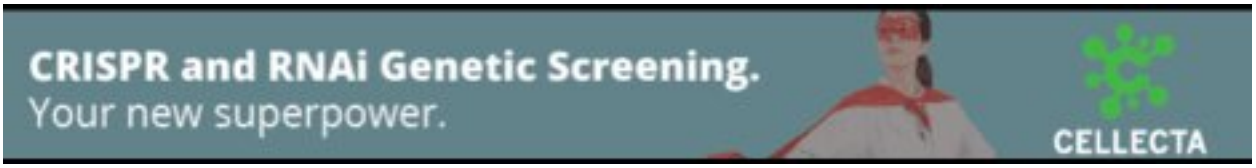

Method

Power-law behavior of transcriptional bursting regulated by enhancer–promoter communication

Zihao Wang,[1,2,3] Zhenquan Zhang,[1,2,3] Songhao Luo,[1,2,3] Tianshou Zhou,[1,2] and Jiajun Zhang[1,2]

[1]*Guangdong Province Key Laboratory of Computational Science, Sun Yat-sen University, Guangzhou 510275, P.R. China;* [2]*School of Mathematics, Sun Yat-sen University, Guangzhou 510275, P.R. China*

Revealing how transcriptional bursting kinetics are genomically encoded is challenging because genome structures are stochastic at the organization level and are suggestively linked to gene transcription. To address this challenge, we develop a generic theoretical framework that integrates chromatin dynamics, enhancer–promoter (E-P) communication, and gene-state switching to study transcriptional bursting. The theory predicts that power law can be a general rule to quantitatively describe bursting modulations by E-P spatial communication. Specifically, burst frequency and burst size are up-regulated by E-P communication strength, following power laws with positive exponents. Analysis of the scaling exponents further reveals that burst frequency is preferentially regulated. Bursting kinetics are down-regulated by E-P genomic distance with negative power-law exponents, and this negative modulation desensitizes at large distances. The mutual information between burst frequency (or burst size) and E-P spatial distance further reveals essential characteristics of the information transfer from E-P communication to transcriptional bursting kinetics. These findings, which are in agreement with experimental observations, not only reveal fundamental principles of E-P communication in transcriptional bursting but also are essential for understanding cellular decision-making.

[Supplemental material is available for this article.]

Gene transcription that is tightly related to three-dimensional (3D) genomic organization is a highly complex and regulated process that shows a discontinuous episodic bursting behavior (Suter et al. 2011; Misteli 2020; Rodriguez and Larson 2020; Tunnacliffe and Chubb 2020). As two cardinal regulatory elements, the promoter and the enhancer are responsible for the accurate spatiotemporal gene expression ensuring reliable cell functioning and cellular decision-making (Zabidi and Stark 2016; Robson et al. 2019; Stadhouders et al. 2019). Many experimental studies have been invested in understanding the roles of distal enhancers in regulating transcriptional bursting kinetics (Bartman et al. 2016; Fukaya et al. 2016; Chen et al. 2018; Rodriguez et al. 2019). However, the mechanism of how 3D chromatin organization (in particular 3D enhancer–promoter [E-P] spatial communication) in one-dimensional time shapes transcriptional bursting patterns still remains elusive.

Hierarchic genomic structures captured by chromosome conformation capture and fluorescence in situ hybridization as well as other experimental technologies have provided evidence for supporting various possible E-P topologies and linking upstream distinctive E-P communications to downstream gene transcription (Ou et al. 2017; Gizzi et al. 2019; Li et al. 2020; Su et al. 2020; Bohrer and Larson 2021). Measurable sustained physical proximity of E-P communication, which is believed to increase the local concentrations of transcription factors (TFs) and coactivators, seems necessary for cells to execute correct gene-transcription programs in living *Drosophila* embryos (Chen et al. 2018; Lim et al. 2018). To understand the mechanism of transcriptional bursting theoretically, many gene models have been proposed, including simple models (e.g., the common ON-OFF model) (Shahrezaei and Swain 2008; Kumar et al. 2014; Corrigan et al. 2016; Zhang and Zhou 2019; Wang et al. 2020) and multistate models that seem good candidates for mimicking complex promoter dynamics in mammalian cells (Harper et al. 2011; Suter et al. 2011; Neuert et al. 2013; Jones et al. 2014; Zhang and Zhou 2014; Rodriguez et al. 2019). However, these models ignore dynamic transcriptional regulation by spatial chromosome topology (Dekker and Mirny 2016; Brouwer and Lenstra 2019; Sood and Misteli 2022). To the best of our knowledge, a comprehensive theory of the information transmission from upstream chromatin organization to downstream transcriptional bursting is still lacking, and important yet fundamental questions such as how E-P communication shapes the observed patterns of mRNA expression and what is the role of the "range of action" for E-P proximity in the control of bursting kinetics remain unsolved. Understanding and revealing transcriptional bursting kinetics characterized by burst size (BS) and burst frequency (BF) require integrative models that consider both 3D chromatin motion (including E-P spatial communication) and upstream-to-downstream regulation.

A collection of experimental evidence has firmly established that the E-P communication strength can significantly raise transcriptional levels (Senecal et al. 2014; Bartman et al. 2016, 2019); for example, the *sna* distal shadow enhancer generates more bursts than the primary enhancer in *Drosophila* embryos (Fukaya et al. 2016). Recent live-imaging measurements have provided clear evidence that E-P genomic distance can effectively control gene activities and thus affect transcriptional bursting kinetics (Fukaya

[3]**These authors contributed equally to this work.**
Corresponding authors: mcszhtsh@mail.sysu.edu.cn, zhjiajun@mail.sysu.edu.cn

Article published online before print. Article, supplemental material, and publication date are at https://www.genome.org/cgi/doi/10.1101/gr.278631.123. Freely available online through the *Genome Research* Open Access option.

34:106–118 Published by Cold Spring Harbor Laboratory Press; ISSN 1088-9051/24; www.genome.org

et al. 2016; Yokoshi et al. 2020; Zuin et al. 2022). These experimental observations indicate that the E-P communication strength limiting the E-P spatial distance and the E-P genomic distance arranged by chromosomal rearrangements are important factors impacting transcriptional bursting patterns. Currently, a new trend is that genomic structures are stochastic at almost every level of organization and that this stochasticity is suggestively linked to gene transcription and finally affects transcriptional outcomes (Hübner et al. 2013; Bohrer and Larson 2021; Sood and Misteli 2022). Given the important impacts of these factors on transcriptional bursting, an unsolved and even theoretically unexplored issue is what principles govern transcriptional bursting kinetics. How E-P spatial and genomic distances differently influence BS and/or BF is not clear either. As a matter of fact, biological systems are by nature multiscale. To date, many experimental studies have shown distinct timescale differences between upstream chromatin dynamics and downstream bursting kinetics (Johnstone et al. 2020; Lammers et al. 2020). For instance, E-P communication occurs on a timescale of seconds to minutes (Chen et al. 2018; Lim et al. 2018; Heist et al. 2019), whereas half-lives of Pol II pause during transcription on a timescale of minutes to hours (Krebs et al. 2017; Shao and Zeitlinger 2017; Henriques et al. 2018). This temporal disconnection between the upstream and the downstream, as well as the stochasticity of genomic organization and transcriptional bursting, lies at the heart of a broad challenge in physical biology of forecasting transcriptional outcomes from the dynamics of underlying molecular processes.

Building upon experimental phenomena and data, we develop a generic theoretical framework to investigate how E-P communication affects transcriptional bursting kinetics, focusing on the uncovering of underlying molecular processes and dynamical mechanisms. This framework, which is formulated as a so-called 4D nucleome equation (similar to the classical differential Chapman–Kolmogorov equation in form) (Gardiner 2004), considers upstream chromatin motion on a fast timescale and downstream mRNA bursty production on a slow timescale, as well as the connection between the upstream and the downstream (see Fig. 1). We use the 4D nucleome equation to analyze dynamic

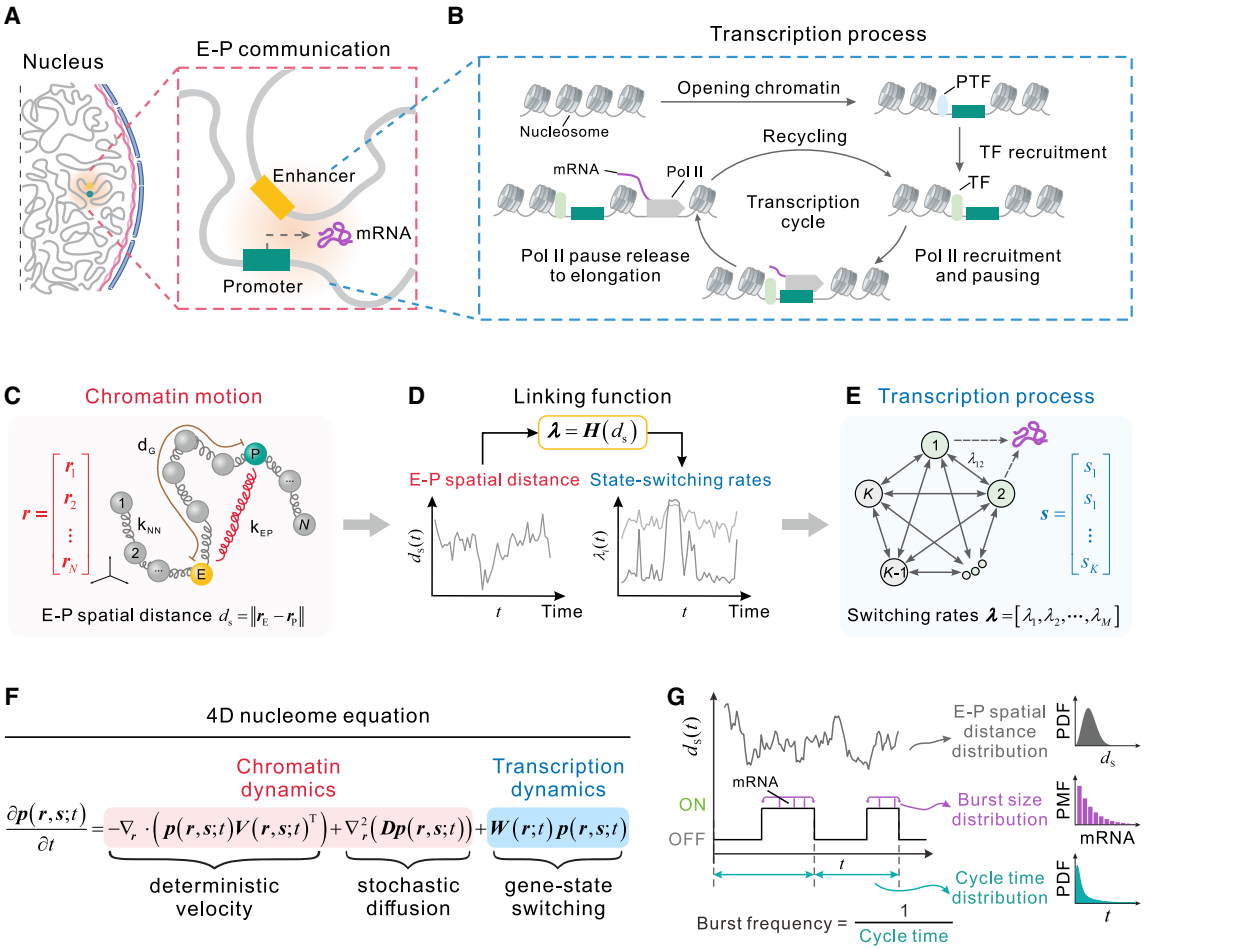

Figure 1. A framework for modeling how E-P communication regulates transcription dynamics. (*A*,*B*) Schematic for a biological model: The upstream E-P communication in the cell nucleus (*A*) guides the downstream transcription, which is a multistep process in which only the main steps are depicted (*B*). (*C*–*E*) Schematic for a physical model: A generalized Rouse model is proposed to model chromatin spatial motion including E-P communication (indicated by the red spring with coefficient k_{EP}), where $\boldsymbol{r} = [\boldsymbol{r}_1, \cdots, \boldsymbol{r}_N]^T$ represents nucleosome positions in 3D (*C*). A link function vector $\lambda = \boldsymbol{H}(d_s)$ bridges the temporal disconnection between the upstream and the downstream (*D*), where d_s is the E-P spatial distance, and $\boldsymbol{H}$ is a Hill-like function vector. (*E*) A schematic of a transcription process, where $\boldsymbol{s} = [s_1, \cdots, s_K]^T$ is the vector of the gene's states, and λ is a vector of state switching rates. (*F*,*G*) Mathematical model: A 4D nucleome equation (*F*) is derived to model the spatiotemporal evolution of the entire system, and the characteristics of the three distributions of interest are schematically shown (*G*).

behaviors of transcriptional bursting across space and time, that is, 4D transcriptional bursting kinetics (Dekker et al. 2017; Marti-Renom et al. 2018). Both model analysis and numerical simulations reveal fundamental principles of the E-P spatial communication in transcriptional bursting, mainly including two universal laws: E-P communication strength up-regulates BF and BS by power laws with positive exponents, and E-P genomic distance down-regulates bursting kinetics by power laws with negative exponents. In addition, we analytically show that E-P spatial distances follow a Maxwell–Boltzmann distribution. The theoretically predicted results are in accordance with experimental data. We emphasize that our model, which shows scalability by interpreting many experimental phenomena reported in the existing literature (Fukaya et al. 2016; Zuin et al. 2022), provides a generic modeling framework for studying how chromatin dynamics affect transcriptional bursting kinetics in realistic cases.

Results

The first principle framework of gene transcriptional bursting

Transcription involving multiple steps is driven mainly by E-P communication (Fig. 1A,B), often showing a burst-like pattern. Our goal is to develop a generic theoretical framework that can reveal the essential mechanism of transcriptional bursting and predict possible dynamic behaviors compatible with experimental observations. This framework considers that upstream chromatin dynamics play on a fast timescale and that downstream transcriptional bursting operates on a relatively slow timescale, but it keeps the upstream and the downstream linked via a biologically reasonable way.

First, based on Figure 1, C through E, we can derive the following 4D nucleome equation (see Methods):

$$\frac{\partial \boldsymbol{p}(\boldsymbol{r}, \boldsymbol{s}; t)}{\partial t} = -\nabla_{\boldsymbol{r}} \cdot (\boldsymbol{p}(\boldsymbol{r}, \boldsymbol{s}; t)\boldsymbol{V}(\boldsymbol{r}, \boldsymbol{s}; t)^{\mathrm{T}}) + \nabla^2_{\boldsymbol{r}}(\boldsymbol{D}\boldsymbol{p}(\boldsymbol{r}, \boldsymbol{s}; t)) + \boldsymbol{W}(\boldsymbol{r}; t)\boldsymbol{p}(\boldsymbol{r}, \boldsymbol{s}; t). \quad (1)$$

Here the column vector $\boldsymbol{p}(\boldsymbol{r}, \boldsymbol{s};t)$ represents the joint probabilities that the positions of N nucleosomes are $\boldsymbol{r}$ and the gene states are $\boldsymbol{s}$ at time t; $\nabla_{\boldsymbol{r}}$ and $\nabla^2_{\boldsymbol{r}}$ are gradient and Laplace operators, respectively; $\boldsymbol{V}(\boldsymbol{r}, \boldsymbol{s};t)^{\mathrm{T}}$ (T: transpose) represents the deterministic velocity field for chromatin spatial motion; $\boldsymbol{D}$ is a diffusion matrix associated with chromatin stochastic motion under isotropic diffusion with diffusional coefficient D; and $\boldsymbol{W}(\boldsymbol{r};t)$ is the nucleosome position–dependent transition matrix for all gene states (Fig. 1F). The first term on the righthand side of Equation 1 represents a deterministic component modeling the upstream chromatin motion, and the second term represents a stochastic component accounting for random fluctuations, both altogether describing the chromatin's spatiotemporal diffusional process. The last term captures the gene states' randomly switching process driven by molecular events such as chromatin remodeling, TF binding, and Pol II clustering. We point out that Equation 1 seems the first theoretical model that comprehensively considers the connection between the upstream and the downstream molecular processes, and can be taken as a good starting point for analyzing how chromatin motion (including E-P communication) affects transcriptional bursting in complex cases.

Second, from a physical viewpoint, upstream chromatin can be modeled as a polymer discretized into a collection of successive monomers connected by harmonic spring (Doi et al. 1988). Both the promoter and enhancer in chromatin are regarded as monomers, and spatial communication exists between them. Chromatin motion involving E-P communication then evolves according to the Langevin equation $\mathrm{d}\boldsymbol{r} = \boldsymbol{V}(\boldsymbol{r}, \boldsymbol{s}; t)\mathrm{d}t + \sqrt{2D}\mathrm{d}\boldsymbol{B}(t)$, which is derived from Equation 1, where $\boldsymbol{B}(t)$ is a vector of independent Brownian motions. We assume that changes in the gene state do not affect chromatin motion. Therefore, $\boldsymbol{V}(\boldsymbol{r}, \boldsymbol{s};t)$ can be approximated as $\boldsymbol{V}(\boldsymbol{r}; t) = -\nabla_{\boldsymbol{r}}U(\boldsymbol{r}; t)/\gamma$, where $U(\boldsymbol{r};t)$ is the total potential of chromatin conformation, and γ is a friction coefficient. $U(\boldsymbol{r};t)$ can be decomposed into $U(\boldsymbol{r};t) = U_{\mathrm{NN}}(\boldsymbol{r};t) + U_{\mathrm{EP}}(\boldsymbol{r};t)$, where $U_{\mathrm{NN}}(\boldsymbol{r};t)$ is the potential for the whole chain and is set as $(1/2)\sum_{j=1}^{N-1} k_{\mathrm{NN}}(\boldsymbol{r}_j - \boldsymbol{r}_{j+1})^2$, with k_{NN} being the common spring coefficient, and $U_{\mathrm{EP}}(\boldsymbol{r};t)$ is the potential for E-P communication and is set as $(1/2)k_{\mathrm{EP}}(\boldsymbol{r}_{\mathrm{E}} - \boldsymbol{r}_{\mathrm{P}})^2$ with E, P $\in \{1, \cdots, N\}$ being the positions of the enhancer and promoter along the DNA line, respectively. Here, k_{EP}, the ratio of the force generated by the biomolecule's interaction involved in E-P communication per unit of E-P spatial distance, represents E-P communication strength, reflecting E-P encounter frequency (Fig. 1C; Supplemental Text A). k_{EP} cannot be directly measured by experiments but can be estimated from experimental data, for example, Hi-C data (Lu et al. 2020). We point out that the Lennard-Jones potential can also be used to simulate E-P communication but does not affect the qualitative results to be obtained (Supplemental Fig. S1F).

Downstream transcription apparatus can be characterized by promoter-state switching (Fig. 1E). To reveal the essential mechanism of how E-P communication regulates transcriptional bursting, we introduce a minimal architecture for gene states—a four-state model (see Methods) (Supplemental Table S1), although more complex architectures are possible. In this model, a deep inactive state (S_{off2}) and a primed but inactive state (S_{off1}), both being integrated as an OFF state, are used to explain chromatin remodeling and TF binding. The Pol II recruitment state (S_{rec}) (Fuda et al. 2009) and Pol II pause release state (S_{rel}) (Chen et al. 2017), two critical processes involved in transcriptional bursting, are taken as an ON state, and mRNA generation is accompanied by the transition from S_{rel} to S_{rec}. If states S_{rel} and S_{rec} switch multiple times during one ON period, transcription will occur in a burst-like manner. The state transition matrix $\boldsymbol{W}$ in Equation 1 consists of gene-state switching rates.

After identifying the above formulations, we build a link in terms of the information flow from upstream to downstream (Fig. 1D), where E-P communication carries the upstream information to orchestrate bursting patterns, and downstream transition rates change accordingly. Specifically, we take E-P spatial distance d_{S} as an input and d_{S}-dependent gene-state switching rates as outputs (see Methods), thus bridging the upstream and the downstream. Although how the ways of E-P communication are implemented is argued (Lim and Levine 2021), E-P proximity has been believed to increase the likelihood of transcription bursting. In general, the smaller the E-P distance is, the larger the switching rates $\lambda = [\lambda_{\mathrm{on1}}, \lambda_{\mathrm{rec}}, \lambda_{\mathrm{rel}}]^{\mathrm{T}}$ are and the smaller the transcriptional termination rates $\lambda' = [\lambda_{\mathrm{off1}}, \lambda_{\mathrm{off2}}]^{\mathrm{T}}$ are. We assume that λ depends on E-P distance and λ' is independent of this distance. Because the Hill function is very successful in modeling biological phenomena (Goutelle et al. 2008), we further suppose that λ is a Hill-like function vector $\boldsymbol{H}$ of d_{S} (see Methods). These assumptions would be idealistic for elaborate organisms, but all the settings constitute an analysis framework, which can be easily extended to more complex cases of transcriptional regulation.

We develop both an effective analytical approach and a numerical simulation algorithm (see Methods) to solve the entire system described by Equation 1. These methods provide a systematic

approach for tracing the respective contributions of the system's key parameters (e.g., E-P communication strength, E-P genomic distances) to the experimentally observable patterns of transcriptional bursting and, further, for revealing the essential mechanism of bursting kinetics.

Distribution characteristics of transcriptional bursting

To see the distribution characteristics of transcriptional bursting kinetics characterized by BS (defined as the number of mRNA molecules produced per burst) and BF (defined as the reciprocal of the cycle time [CT] that is defined as the total time that the gene dwells at OFF and ON states), we mainly find the BS distribution $p_{BS}(m)$ and the CT distribution $p_{CT}(t)$. Note that BS and CT depend on the E-P spatial distance d_S, which is a random variable following the distribution denoted by $p_{DS}(d_S)$ (Fig. 1G). Before presenting results on $p_{BS}(m)$ and $p_{CT}(t)$, we derive the expression of $p_{DS}(d_S)$.

We analytically find that d_S obeys the following exact Maxwell–Boltzmann distribution (see Supplemental Text B; Supplemental Fig. S1A)

$$p_{DS}(d_S) = \sqrt{\frac{2}{\pi}}\Theta^{-3} d_S^2 \exp\left(-\frac{d_S^2}{2\Theta^2}\right), \tag{2}$$

where $\Theta = \sqrt{D\gamma(k_{NN}/d_G + k_{EP})^{-1}}$, which is a compound parameter depending on the genomic property, clearly defines an analytical relationship between E-P spatial distance d_S and the E-P communication parameters (including E-P communication strength k_{EP} or E-P genomic distance d_G). The term $k_{NN}/d_G + k_{EP}$ actually represents the integrative effect of two paralleling springs, possibly hinting the principle of engineering communication between regulatory elements. Quantitative measurements of the distance between *Sox2* and its essential enhancer in living mouse embryonic stem cells (Supplemental Fig. S1B; see Alexander et al. 2019) and the distance between the *eve* locus and its enhancer in fly embryo (Brueckner et al. 2023) have indicated the validity of this Maxwell–Boltzmann distribution. Equation 2 also uncovers a power-law behavior between encounter probabilities and E-P spatial (or genomic) distance, which is in accordance with experimental data for consecutive and nonconsecutive TAD borders in *Drosophila* (Supplemental Fig. S1E; see Cattoni et al. 2017).

We can also derive the expressions of two distributions $p_{BS}(m)$ and $p_{CT}(t)$ (for details, see Methods). Then, we find that if the gene-state switching rates are independent of d_S, BS follows a geometric distribution with the characteristic parameter representing the success probability of burst termination (Supplemental Text B); The duration of the OFF period follows a biexponential distribution (Supplemental Text B), supporting that gene activation is not necessarily a one-step process following an exponential distribution (Harper et al. 2011; Suter et al. 2011; Kandhavelu et al. 2012). In addition, the CT distribution is the weighted combination of multiple exponential distributions (Supplemental Text B), which shows a nonorigin peak. If the gene-state switching rates depend on d_S, $p_{BS}(m)$ or $p_{CT}(t)$ has no analytical expression but has an exactly approximate expression, that is, Equation 12 in the Methods, which is derived by a timescale separation method that is owing to the fast chromatin motion and the slow transcription reactions (Thomas et al. 2014).

We point out that in both cases, our approaches for deriving the analytical expressions of $p_{BS}(m)$ and $p_{CT}(t)$ can be applied to other more complex gene-transcription models. Thus, all qualitative results are universal. In addition, parameter settings for the results showed in the following several subsections are put in Supplemental Table S2. Some parameters (e.g., those related to chromatin motion) are determined directly based on biological processes and physical equations, and others (e.g., transcriptional rates) are chosen based on theoretical analysis results and actual biological time scales (Supplemental Text F).

Transcriptional bursting kinetics follow power laws

How E-P communication modulates BS and BF is not only a debated biological issue but also an unsolved theoretical issue. Here, we use the above arsenal of theoretical analysis to explore the qualitative impact of E-P communication strength k_{EP} on transcriptional bursting kinetics (i.e., BS and BF). As one of the most common modular organisms, *Drosophila* has been extensively studied in terms of bursting (Jennings 2011; Douglas 2018). Indeed, distinctive enhancers such as *sna* shadow and *sna* primary enhancer in *Drosophila* that interact with cognate promoter may lead to different burst kinetics (Perry et al. 2010; Bothma et al. 2015; Fukaya et al. 2016). In our analysis, we take different values of k_{EP} to characterize the inherent behaviors of E-P interaction. Meanwhile, we make use of the fact that effective experimental means such as external hormone (Stavreva et al. 2015) or heavy metal stimulations (Murata et al. 1999) can make E-P communication stronger; that is, k_{EP} becomes larger. To reveal the distinct effects of different k_{EP} on bursting kinetics, we keep the E-P genomic distance fixed (Fig. 2A).

Figure 2B depicts how changes in k_{EP} alter chromatin conformations and further affect bursting profiles. Theoretically, a larger (smaller) k_{EP} corresponds to a shorter (longer) E-P spatial distance, and then the increasing k_{EP} can boost both BS and BF (Supplemental Figs. S1C, S4A,B). These features have been qualitatively supported by experimental evidence from different organisms (Bartman et al. 2016; Fukaya et al. 2016; Fritzsch et al. 2018; Bartman et al. 2019). Because the ON state dwell-time remains fundamentally the same, the amplified BF can be achieved by progressively reducing the OFF state dwell-time (Supplemental Fig. S4C,D; Larson et al. 2013; Fritzsch et al. 2018; Rodriguez et al. 2019). This implies that the gene-state switching rate λ_{on1}, associated with TF recruitment in biology, is a principal parameter affecting BF, in agreement with the experimental finding that a higher TF level leads to a higher BF on the *FOS* (also known as *c-Fos*) gene (Senecal et al. 2014).

To reveal the qualitative relevance of bursting kinetics to E-P communication strength, we further analyze two logarithmic gains $\partial\log_{10}\mathrm{BS}/\partial\log_{10}k_{EP}$ and $\partial\log_{10}\mathrm{BF}/\partial\log_{10}k_{EP}$ (i.e., two partial derivatives), which measure how BS and BF are affected by k_{EP}. Binary approximations of gene-state switching rates provide a good strategy for simplifying analysis including estimating BS and BF (see Methods) (Supplemental Fig. S5D,E). The detailed theoretical analysis shows that the logarithmic gains are about zero when k_{EP} is too small ($k_{EP} < 0.01$) or too large ($k_{EP} > 1$) (Supplemental Fig. S5A–C), implying that the transcriptional burst response is insensitive to k_{EP} in these two cases. Then, we focus on a reasonable biological range of k_{EP} (e.g., $0.01 < k_{EP} < 1$). The logarithmic gains are almost constant, and BS and BF can be thus approximated with linear functions of k_{EP} on a logarithmic scale (Fig. 2C,D; Supplemental Fig. S5D,E). Concretely, for $0.01 < k_{EP} < 1$, BS and BF approximately obey the following power-law behaviors

$$\text{burst size} \sim (k_{EP})^{S_{BS}},\ \text{burst frequency} \sim (k_{EP})^{S_{BF}}, \tag{3}$$

where S_{BS} and S_{BF} are two positive scaling exponents that can be theoretically estimated (see Methods). Note that these two different scaling exponents, for example, $S_{BS} = 0.23$ in Figure 2C and

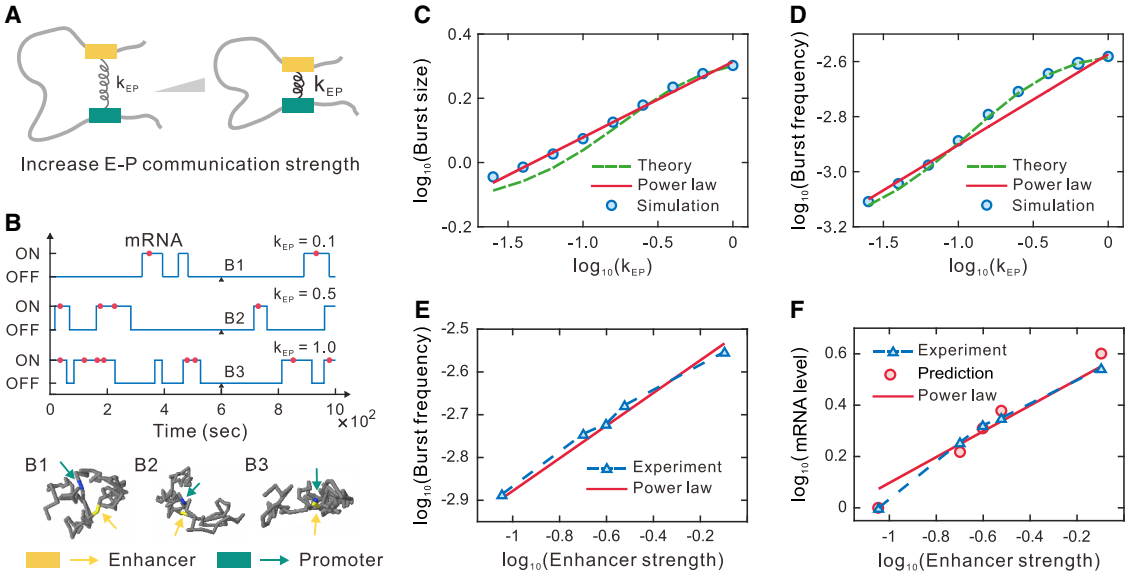

Figure 2. Effect of the E-P communication strength on transcriptional bursting kinetics. (*A*) Schematic illustration of the augment of E-P communication strength k_{EP}. (*B*) Example traces of binarized transcriptional activity for three different values of k_{EP}, where red points represent the mRNA generation events, and the corresponding 3D chromatin structures are shown on the *bottom*. (C) Log–log plot for the relationship between mean burst size and strength k_{EP}. The green dashed line represents the theoretical result, whereas blue circles show numerical simulations. The red solid line indicates a power-law approximation (Equation 3) with a scaling exponent, $S_{BS} = 0.23$. (*D*) Log–log plot for the relationship between burst frequency and k_{EP}. Meanings of symbols are the same as those in *C*, but the scaling exponent is $S_{BF} = 0.33$. (*E*,*F*) Log–log plot of experimental data from Fukaya et al. (2016). The *x*-axis shows the E-P communication strengths of different enhancers, obtained by theoretical inferring based on the burst frequency data (converted the unit into sec^{-1}). The red points in *F* represent the theoretical result of mRNA level (converting its trend of change into a fold change), whereas the blue dashed line shows the experimental data (fluorescence intensity is a relative value, converting its trend of change into a fold change).

$S_{BF} = 0.30$ in Figure 2D, are critical indices because they reflect the ability of BS and BF responses to E-P communication, which will be analyzed in detail in the next section. To ascertain whether the power-law behaviors shown in Equation 3 always hold, we change key parameters in broad ranges. For all possible cases of parameter values, we find that log–log plots between BS (or BF) and k_{EP} still show an approximately linear relationship, implying that the growing tendency can still be featured by power-law relationships (Supplemental Fig. S6).

The above theoretical predictions have been verified by experimental data. Based on the BF data (converting the unit into sec^{-1}) for different enhancers in living *Drosophila* embryos (Fukaya et al. 2016) and the above model, we theoretically infer the E-P communication strength for each enhancer and calculate the mean mRNA (which approximately equals to the product of BS and BF) (Li et al. 2021). We find that the mRNA level matches well with the experimental results (fluorescence intensity is a relative value, converting its trend of change into a fold change), and both the BF and mRNA levels show power-law relationships in logarithmic coordinates (Fig. 2E,F). Our results not only show the ability of our model in explaining and predicting the experimental data but also prove the validity of the power-law theoretical results.

E-P communication mainly modulates BF rather than BS

Note that Equation 3 indicates that BS and BF regulated by E-P communication strength k_{EP} follow their own power-law behaviors. Because S_{BS} and S_{BF} in Equation 3 reflect the regulation ability of k_{EP}, we next compare the sizes of S_{BS} and S_{BF}, that is, compute the ratio of S_{BF}/S_{BS}, to show which of the BS and BF is primarily regulated by E-P communication. For this goal, we change E-P communication strength and all gene-state switching rates in broad ranges. In general, extracting insights from directly analyzing the effects of these changes in high-dimensional parameter space consisting of E-P communication strength and all gene-state switching rates on BS and BF is very difficult. Therefore, we resort to a dimension reduction method that maps a high-dimensional parameter space into an experimentally measurable and theoretically computable two-dimensional space (Fig. 3A) in which two indices ρ_{BS} and ρ_{BF} are defined as the ratios of the maximum BS and BF over the minimum BS and BF, respectively (see Supplemental Text D).

Next, we calculate ratio S_{BF}/S_{BS} in the (ρ_{BF}, ρ_{BS}) space. Note that one point in the low-dimensional space possibly corresponds to multiple points in the high-dimensional space owing to the irreversibility of the mapping. To overcome this multiple-to-one difficulty, we use the averaging method to estimate the ratio S_{BF}/S_{BS} and then find that this ratio generally increases with the growth of ρ_{BF} or with the shrinking of ρ_{BS} (Fig. 3A; Supplemental Fig S7A). In Figure 3B, the separatrix $S_{BF}/S_{BS} = 1$ (red line) separates the space into two regions: upper $S_{BF} > S_{BS}$ and lower $S_{BF} < S_{BS}$. In particular, the data shown in Figure 2, C and D, correspond to the point $(\rho_{BF}, \rho_{BS}) = (5.8, 3.1)$, which apparently locates in the area of $S_{BS} < S_{BF}$ ($S_{BF}/S_{BS} = 1.4$) (Fig. 3B, red-blue mixed circle). To show the reliability of this averaging method, we use the minimum (or maximum) value rather than the mean to compute S_{BF}/S_{BS}. As a result, the separatrix $S_{BF}/S_{BS} = 1$ displays a similar changing trend; that is, the range of the ρ_{BS} satisfying $S_{BS} < S_{BF}$ gradually becomes larger with the increase of ρ_{BF} (Supplemental Fig. S7B).

To complete the above analysis, we consider enhancer deletion where k_{EP} is exactly zero (Supplemental Fig. S2A). For the same parameter values as in the above calculation, we find that the sizes of ρ_{BS} and ρ_{BF} with enhancer deletion are the same as those with enhancer regulation, but the slope ratio $S^E_{BF}/S^E_{BS} (= 1.56)$ (representing the ratio after enhancer deletion)

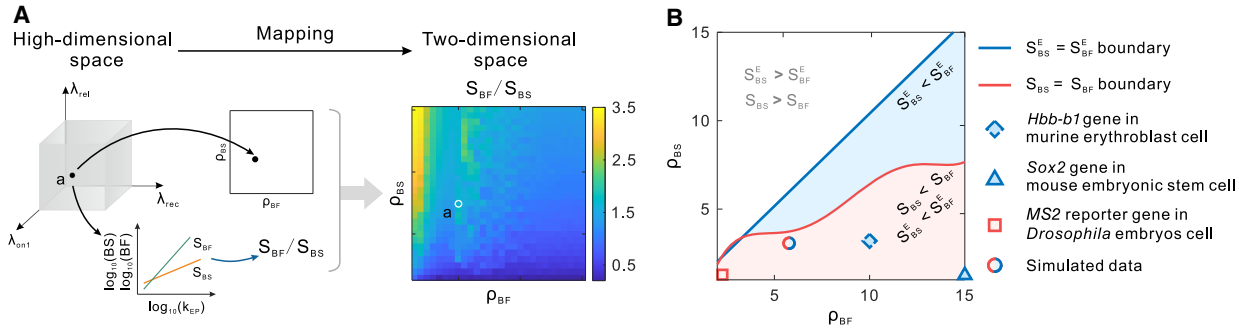

Figure 3. Separatrixes for power-law behaviors of BS and BF in the (ρ_{BF}, ρ_{BS}) plane. (*A*) Schematic illustration of the dimension reduction method, in which a high-dimensional parameter space is mapped into the (ρ_{BF}, ρ_{BS}) space, and the calculated values of S_{BF}/S_{BS} (the *bottom inset*) are plotted in the (ρ_{BF}, ρ_{BS}) plane (the heatmap). (*B*) The red line stands for the boundary obtained by smoothing the theoretical results S_{BF}/S_{BS}; the blue line, for the boundary obtained by smoothing the theoretical results S^E_{BF}/S^E_{BS} (after enhancer deletion). The colored regions indicate that E-P communication affects BF more than BS under different situations. The square at point (2.3, 1.3) corresponds to the MS2 reporter gene in *Drosophila* embryos cell in work of Fukaya et al. (2016), the triangle at point (15, 1.4) to the *Sox2* gene in mouse embryonic stem cell in work of Larsson et al. (2019b), the dashed diamond at point ($\cdot$, 3.3) to the *Hbb-b1* (hemoglobin, beta) gene in murine erythroblast cell in work of Bartman et al. (2016), and the red blue mixed circle to the simulated data. Note that the burst frequency in work of Larsson et al. (2019b) defined as the reciprocal of OFF state dwell-time, which is approximately converted to the reciprocal of CT, and that the ρ_{BF} at the dashed diamond point ($\cdot$, 3.3) related to burst fraction in work of Bartman et al. (2016) is approximate. By the blue region, we mean the whole area *below* the blue line (some part is covered by red regions).

(Supplemental Text D) is different from the value of $S_{BF}/S_{BS}(=1.4)$ (Fig. 3B, red-blue mixed circle). Using the results obtained by a similar method of calculating S_{BF}/S_{BS}, we draw the separatrix $S^E_{BF}/S^E_{BS}=1$ in Figure 3B (blue line). Then, we find that whether the enhancer deletion is considered does not influence ρ_{BS} and ρ_{BF} but impacts ratios S_{BF}/S_{BS} and S^E_{BF}/S^E_{BS} (referring to two different oblique lines in Supplemental Fig. S2F).

Finally, we locate the experimental data into the (ρ_{BF}, ρ_{BS}) space and determine which of BS and BF is mainly regulated by E-P communication. Although experimental data on gene-state switching rates are lacking, we may use the maximum and minimum BS and BF experimentally available to compute ρ_{BS} and ρ_{BF}. Because we integrate the model parameters into two experimentally measurable and theoretically computable quantities, the validation of model predictions does not require a specific data set. Based on the analysis of data from transgene experiments, we find that the MS2 reporter gene displays different bursting kinetics for different enhancer strengths; for example, for a stronger *sna* shadow enhancer and a weaker *Kr* CD2 enhancer, the result is (ρ_{BF}, ρ_{BS}) = (2.3, 1.3) (Fig. 3B, red square point; Fukaya et al. 2016). The maximum BS of the gene *Hbb-b1* (hemoglobin, beta) measured in an experiment of erythroid maturation is over three times the minimum gained by the deletion of the LCR enhancer (Fig. 3B, dashed blue diamond point; Bartman et al. 2016). In addition, based on the *Sox2* gene expression data with and without enhancer deletion in normal ES cells, we can infer that the BS reduces 1.4 times and the BF reduces roughly 15 times (Fig. 3B, blue triangle point; Larsson et al. 2019b). We find that all these analyzed experimental data are all located in a narrower region of $S_{BS}<S_{BF}$ (the right lower region in Fig. 3B), further verifying that the E-P communication mainly modulates BF rather than BS.

Saturation effects of E-P genomic distance on bursting kinetics

Having delved into the qualitative effect of E-P communication strength k_{EP} on bursting kinetics as described in Equation 3, we next analyze how the E-P genomic distance d_G quantitatively impacts transcriptional activities and further bursting kinetics. To focus on the effect of d_G on BS and BF, we freeze k_{EP} but make d_G increase. This can be achieved by arranging the enhancer and the promoter symmetrically on the chain and letting them move in the opposite direction along the chain (Fig. 4A).

From Equation 2, we see that d_G and k_{EP} have the opposite impact on E-P spatial distance (Supplemental Fig. S1C). By the similar method of analyzing the effect of k_{EP} on BS and BF, we find that the two logarithmic gains $\partial\log_{10}\mathrm{BS}/\partial\log_{10}d_G$ and $\partial\log_{10}\mathrm{BF}/\partial\log_{10}d_G$ are negative, implying that the increasing E-P genomic distance can reduce BS and BF (Supplemental Fig. S5F–H). With the further increase of d_G, both BS and BF finally reduce to constants. These analyses indicate that the responses of BS and BF to the E-P genomic distance show first descent and then stable change tendencies if other system parameters are fixed (Fig. 4B,C).

To confirm the saturation effects obtained by the above theoretical analysis, we first carry out numerical simulations and then perform the Kruskal–Wallis nonparametric test for simulated samples. This statistical test can identify the turning point of the responses of BS and BF to d_G. Here, the turning point (Fig. 4B,C, black dashed lines) is defined as the value of d_G for which the Kruskal–Wallis test has no significant difference for the first time (Fig. 4B,C, gray circles). We denote the d_G values corresponding to the turning points of BS (BF) as d_G^{BS} (d_G^{BF}).

Furthermore, we use functions to characterize the above saturation effects. The logarithmic gains of BS and BF are almost constant for d_G in the range of $d_G \le d_G^{BS}$ or $d_G \le d_G^{BF}$, implying that in this range, the logarithmic gains can be approximated as linear functions of d_G, or equivalently, BS and BF can be approximated as power functions of d_G with the exponents ℓ_{BS} and ℓ_{BF}, respectively (Supplemental Fig. S5I,J). In contrast, BS and BF are all constants in the range of $d_G > d_G^{BS}$ or $d_G > d_G^{BF}$. In summary, the change tendencies of BS and BF can be mathematically described as

$$\text{burst size} \sim \begin{cases} (d_G)^{\ell_{BS}}, & d_G \le d_G^{BS}, \\ const., & d_G > d_G^{BS}, \end{cases}$$
$$\text{burst frequency} \sim \begin{cases} (d_G)^{\ell_{BF}}, & d_G \le d_G^{BF}, \\ const., & d_G > d_G^{BF}. \end{cases} \quad (4)$$

Here ℓ_{BS} and ℓ_{BF} are two negative scaling exponents that can be theoretically estimated. Note that these scaling exponents are in general different between BS (e.g., $\ell_{BS}=-0.16$ in Fig. 4D, red)

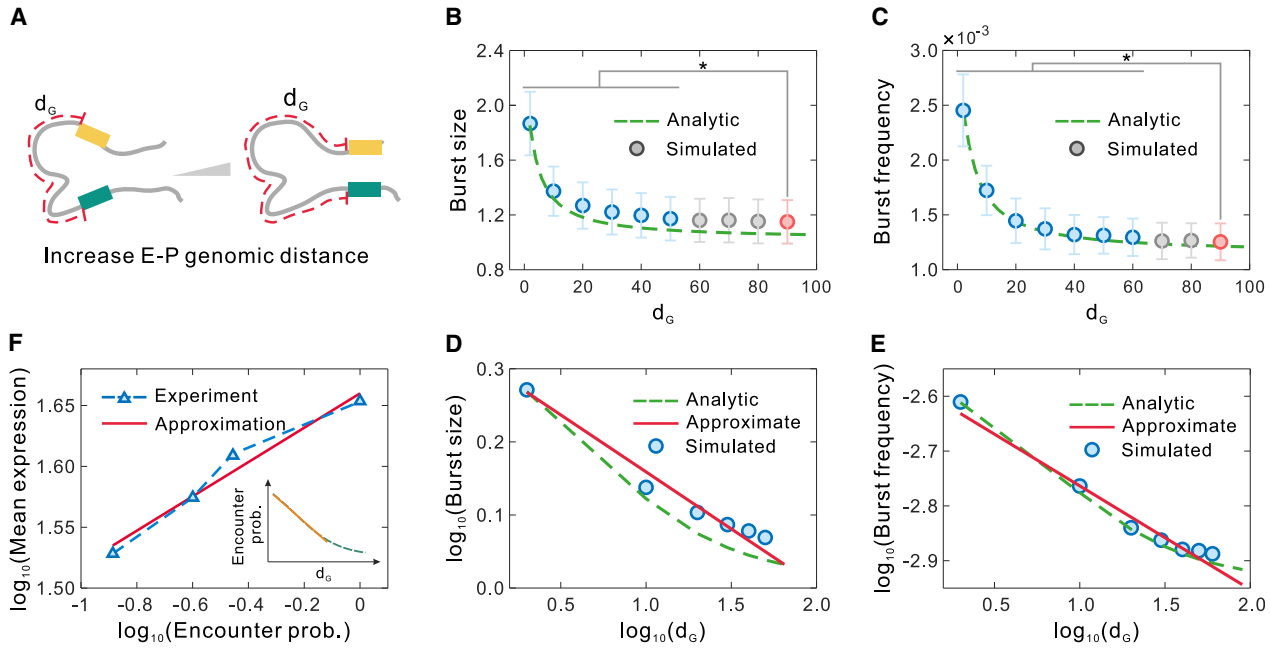

Figure 4. Effect of E-P genomic distance on transcriptional bursting kinetics. (*A*) A schematic diagram shows the increment of E-P genomic distance d_G. (*B*) Influence of d_G on burst size. Dashed green line represents the theoretical result, whereas circles show numerical simulations. The blue circles indicate significant differences compared with the end data point (red) via Kruskal–Wallis nonparametric test, and the gray circles indicate no significance. (*C*) Influence of d_G on burst frequency, where the meanings of all symbols are the same as those in *B*. (*D*) Log–log plot shows the relationship between mean burst size and d_G. Blue circles are the data points with significant differences in *B*. The red solid line indicates the power-law approximation (Equation 4) with the scaling exponent $\ell_{BS} = -0.16$. Meanings of the symbols are also similar to those in *B*. (*E*) Log–log plot shows the relationship between burst frequency and d_G. Meanings of the symbols are similar to those in *D*, but the scaling exponent is $\ell_{BF} = -0.19$. (*F*) Log–log plot of experimental data from Zuin et al. (2022). *Inset* shows the log–log relationship between d_G and encounter probability. The yellow line indicates an approximate power-law relationship for smaller d_G.

and BF (e.g., $\ell_{BF} = -0.19$ in Fig. 4E, red). An intuitive explanation for the asymptotic trend in large d_G is that the lumping parameter $\Theta = \sqrt{D\gamma(k_{NN}/d_G + k_{EP})^{-1}}$ in Equation 2 approaches to a constant with the enlargement of d_G, indicating that for sufficiently large d_G, the effect of E-P communication on transcriptional bursting is mainly determined by communication strength k_{EP} rather than by E-P genomic distance d_G.

The above saturation effects have been also verified by experimental results. First, quantitative live-cell imaging methods showed that a large E-P genomic distance between the *sna* shadow enhancer and its target gene significantly diminishes the levels of BS and BF in *Drosophila* (Fukaya et al. 2016; Yokoshi et al. 2020), in accordance with our prediction on what BS and BF are monotonically decreasing with increasing d_G. Second, the mRNA expression level, which approximately equals the product of BS and BF (Li et al. 2021), is an approximate linear function of a smaller E-P genomic distance d_G on a logarithmic scale (Fig. 4F; Zuin et al. 2022). Third, now that a monotonically decreasing transcription level does not drop to zero, the case that the level remains at a low level for large d_G could happen (Zuin et al. 2022). In a word, the E-P genomic distance impacts the mRNA expression level in a piecewise power manner as described in Equation 4.

Mutual information reveals the dependence of bursting kinetics on E-P communication

In the above sections, we have used the average method, that is, calculating the mean BS and BF (the reciprocal of mean CT) that only consider the mean information of BS's and CT's distribution, to study the impact of E-P communication on bursting kinetics. Here, we investigate bursting kinetics from a perspective of information transmission. The signaling pathway of transcriptional regulation transmits the upstream E-P communication signal distribution $p_{DS}(d_S)$ to the downstream transcriptional output distribution $p_X(x)$ (Fig. 5A). The noisy "promoter channel" limits the fidelity of this information transduction. To better understand the ability of E-P communication to regulate BS and BF, here we use Shannon mutual information to measure how much information about the E-P communication is decoded in bursting kinetics (Shannon 1948; Cover 1999). Mutual information MI(*X*, *DS*) measured in bits is defined as

$$\mathrm{MI}(X, DS) = \int_0^{+\infty}\int_0^{+\infty} p_{X,DS}(x, d_S)\log_2\left(\frac{p_{X,DS}(x, d_S)}{p_X(x)p_{DS}(d_S)}\right)\mathrm{d}x\mathrm{d}d_S, \quad (5)$$

where $p_X(x)$ can represent BS distribution $p_{BS}(m)$, CT distribution $p_{CT}(t)$, OFF dwell-time distribution $p_{OFF}(t)$, and ON dwell-time distribution $p_{ON}(t)$, respectively (Supplemental Fig. S4). The mutual information defined in such a manner can capture the contributions of all the aspects of transcriptional output distributions, not just the mean values.

Based on the computation of MI(*X*, *DS*) in a wide range of k_{EP}, we find that MI(*BS*, *DS*) is much smaller than MI(*CT*, *DS*) (Fig. 5B, C), implying that BF transmits more information than BS. Moreover, MI(*ON*, *DS*) is two orders smaller than MI(*OFF*, *DS*), indicating that ON dwell-time is insensitive when responding to the transduced information (Fig. 5C, red dashed line). Additionally, all the MI(*X*, *DS*) in Figure 5, B and C, show first an increase and then a decrease, indicating that the information transduction capacity is

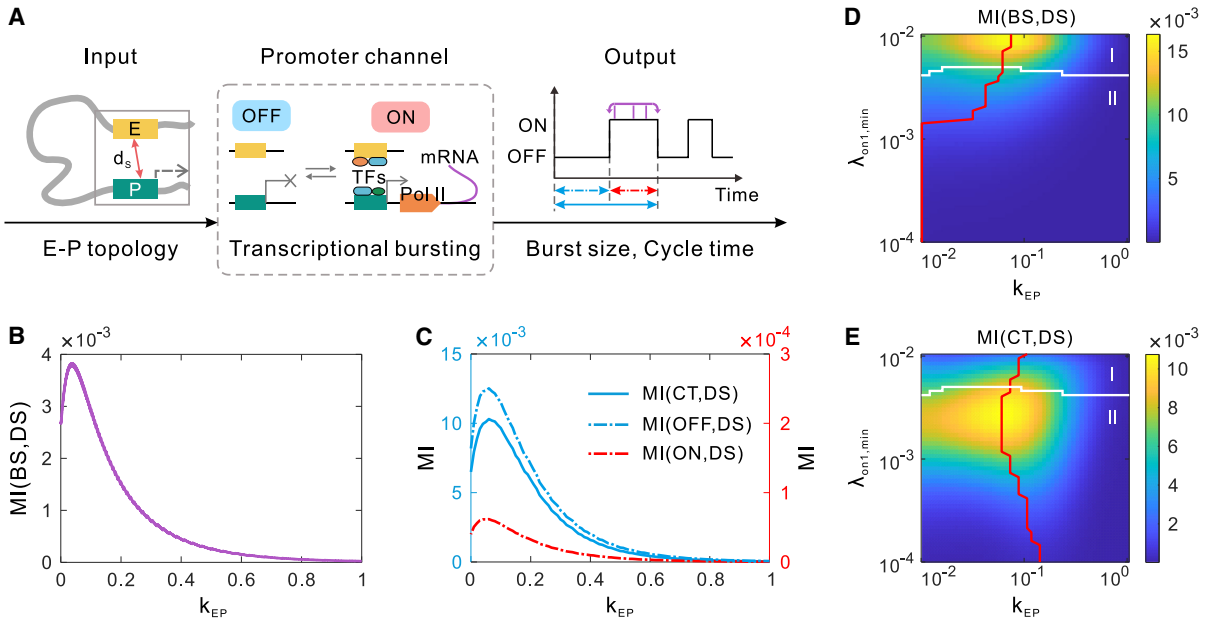

Figure 5. Mutual information reveals the effect of E-P communication on bursting kinetics. (*A*) An information theoretic framework is used to study the effect of input E-P topology on bursting output. The promoter governing transcriptional bursting can be considered a noisy channel. (*B*) Mutual information between E-P spatial distance and burst size (MI(*BS*, *DS*)) as a function of E-P communication strength k_{EP}. (*C*) Mutual information between E-P spatial distance and cycle time (or OFF time, ON time) as a function of k_{EP}. (*D*,*E*) Heatmap shows the effect of k_{EP} and minimum rate $\lambda_{on1,min}$ on MI(*BS*, *DS*) (*D*) and on MI(*CT*, *DS*) (*E*). The red line shows the values of k_{EP} obtained from the MMIs with different $\lambda_{on1,min}$. The white line is the separatrix between the values of MI(*BS*, *DS*) and MI(*CT*, *DS*). Region I stands for MI(*DS*, *BS*) > MI(*DS*, *CT*); region II, for MI(*DS*, *BS*) < MI(*DS*, *CT*).

tunable and that there exists an optimal k_{EP} that maximizes the MI (*X*, *DS*).

Note that the maximum mutual information (MMI) measures the maximum information transmission capacity over all possible signal distributions. Obviously, the MMI exists in Figure 5, B and C, where $k_{EP} = 0.05$ for MI(*BS*, *DS*) and $k_{EP} = 0.07$ for MI (*CT*, *DS*). To ascertain whether or not such an optimal k_{EP} always exists, we change key parameters in wide ranges and find that there is indeed a critical k_{EP} maximizing the MI(*X*, *DS*) shown in Figure 5, D and E, and Supplemental Figure S8. In addition, the MMIs for BS and CT correspond to different k_{EP} values (Fig. 5D,E, red lines). This asynchronous maximization indicates that the signal transduction pathway is BS or BF specific. In particular, the observation that MI(*DS*, *BS*) is smaller than MI(*DS*, *CT*) in region II (Fig. 5D,E, the region below the white line) indicates that BF transmits more E-P communication information than BS, and consequently, E-P communication mainly regulates BF rather than BS.

Discussion

Imaging studies, high-resolution chromatin conformation maps, and genome-wide occupancy profiles of architectural proteins have revealed that genome topology encoding E-P communication information is tightly correlated with gene expression through complex regulatory layers, creating various possible transcriptional burst phenotypes. The prediction of these phenotypes requires a quantitative understanding of transcriptional bursting mechanisms underlying the influence of genomic architectures. In this paper, we have proposed a multiscale model, which integrates the 3D information on chromatin dynamics into transcription bursting, to shed light on the pivotal role of E-P spatial communication in the control of transcriptional bursting kinetics.

We have established a generic modeling framework that captures salient features of intra-nuclear transcriptional bursting processes. First, we use the generalized Rouse model, which can well describe chromatin motion including E-P communication, to model chromatin dynamics. Second, we use a four-state model of gene transcription to capture important events occurring in transcriptional processes. A special feature of our model is that it uses a change of gene state to model the simultaneous freeing of promoter sites and the production of mRNA owing to unpausing of the promoter-proximal paused state (Cao et al. 2020; Karmakar 2020; Braichenko et al. 2021; Karmakar and Das 2021; Szavits-Nossan and Grima 2023; Weidemann et al. 2023). This is crucial for capturing the feature that only one Pol II is permitted to bind to promoter, and the second Pol II recruitment must occur after the first Pol II pause release. Also, our model can capture some characteristics (such as traveling ratio, the effect of altering Pol II pause release rate) that cannot be obtained by the previous models. Third, we use a function vector to link upstream chromatin configurations to downstream gene transcription. The function vector can be viewed as an information transmission process, which can be sensitive, insensitive, positively correlated, or negatively corrected. Different link functions can result in the distance being irrelevant or even anticorrelated with transcription to characterize distinctive experimental phenomena (Benabdallah et al. 2019). It is worth pointing out that more complex E-P topologies, transcription processes, or/and link functions can be incorporated in our model, but the qualitative (but possibly quantitative) results, including power-law behaviors and the preferential modulation of BF showed by theoretical derivation, still hold.

Our analysis has given a clear answer to the question of whether BS or BF is modulated more than the other by E-P communication. In contrast to the transcriptome-wide inference that

shows the important role of E-P communication in controlling BF (Larsson et al. 2019a,b; Ochiai et al. 2020), we have theoretically confirmed that enhancer mainly modulates BF rather than BS (Fig. 3B), which is in agreement with observations of most experiments (Walters et al. 1995; Sutherland et al. 1997; Larson et al. 2013; Bartman et al. 2016; Fukaya et al. 2016; Zuin et al. 2022). Moreover, we have given theoretical estimates on the effect of the enhancer on BF and BS, which is based on directly calculating the ratio of the maximum and minimum values of BS and BF experimental data available. In addition, from the view of mutual information, we have shown that transcriptional bursting kinetics are regulated by transmitting more information to BF, which further verifies the importance of enhancers in modulating BF.

Our results allow us to make important predictions about how upstream chromatin dynamics affect downstream transcriptional bursting kinetics. First, we have shown that E-P communication strength k_{EP}, a key parameter in our model, up-regulates BS and BF in power-law manners with positive exponents. These power-law behaviors were verified by experimental data (Fukaya et al. 2016), and more experiments are still needed. Second, we have shown that the E-P genomic distance d_G, another vital parameter in our model, modulates BS and BF in saturating fashions. These saturation effects were also verified by recent experimental observations (Zuin et al. 2022). The opposite change trends for the effects of k_{EP} and d_G on bursting kinetics showed that the combination of k_{EP} and d_G would be a flexible regulation strategy that can provide insights into complex mechanisms of biological processes in organisms. In addition, the fact that different gene-state transition rates lead to different scaling exponents in power-law behaviors of BS and BF indicates that the regulatory logics shaping differential signal transduction pathways would be cell specific and even gene specific (Brivanlou and Darnell 2002). Third, using mutual information to measure how upstream E-P communication dynamically and stochastically regulates downstream transcriptional bursting kinetics would be a more reasonable way. We have shown that the promoter information transduction capacity is tunable, and the MMI can be obtained by adjusting the E-P communication strength k_{EP}. Supplemental Text E gives the possible reasons for the small value of mutual information.

Recently, Xiao et al. (2021) and Zuin et al. (2022) studied the control of 3D structure (including E-P communication) to gene transcription in different manners. The former assumed that the E-P signal participated in the accumulation and removal of TFs conducive to transcription while ignoring the actual chromatin conformation. The latter used two discrete states (far and close) rather than a continuous random variable, as considered in our model, to simulate the E-P interaction and impact the OFF to ON process in a multistep process with cumulative effects. Our model's direct and dynamic regulation leads to the variable rate from S_{off2} to S_{rec}, which can basically be considered an alternative way to the cumulative effect process. Thus, our model explicitly considered the continuous fluctuation of upstream chromatin and the discrete switching of promoter states in the 4D space.

Our results are not limited to specific genes in *Drosophila* but may be applied to other organisms. The experimental data from different organisms such as a mouse model can be also well fitted (Figs. 3, 4F; Bartman et al. 2016; Zuin et al. 2022), indicating the extensibility of our results. Owing to the lack of experimental data on chromatin conformation and transcription burst data of the same gene in different situations, more experiments are needed to confirm the theoretical predictions. Our modeling framework can also be extended to more complex situations. For example, some experimental studies reported that transcription can affect chromatin structure (Busslinger et al. 2017; Heinz et al. 2018), and we can incorporate this feedback to our model by modifying the gene-state-dependent drift function $\boldsymbol{V}(\boldsymbol{r}, \boldsymbol{s};t)$ in Equation 1. In addition, our modeling of chromatin motion is not limited to one-pair E-P communication. The potential applications may include the cases of multiple enhancers to one promoter (He et al. 2014), one enhancer to multiple promoters (Fukaya et al. 2016), or superenhancers (Pott and Lieb 2015). Using multistate models of gene expression to extract insights from vast experimental data and complex biological phenomena is imperative. Our four-state model is not a default option, and we may adjust the form of the downstream transcription model to include more complex biological processes, such as mRNA splicing (Kan et al. 2002) and cell cycle (Johnson and Walker 1999).

Finally, we point out that our theoretical model, which aims to develop a general modeling framework to study 4D transcriptional bursting kinetics, may provide an opportunity for a dialog between theoretical studies and biological experiments. We envision that our modeling framework will be useful for biophysical analysis of broader in vivo cellular processes.

Methods

Derivation of 4D nucleome equation

Let $\boldsymbol{p}(\boldsymbol{r}, \boldsymbol{s};t)$ be a vector of the joint probability density functions (PDFs) that nucleosomes are in position $\boldsymbol{r}=[\boldsymbol{r}_1, \cdots, \boldsymbol{r}_N]^T$ and the gene is in state $\boldsymbol{s}=[s_1, \cdots, s_K]^T$ at time t, where T is transpose. Note that $\boldsymbol{p}(\boldsymbol{r}, \boldsymbol{s};t)=[\boldsymbol{p}(\boldsymbol{r}, s_1;t), \cdots, \boldsymbol{p}(\boldsymbol{r}, s_K;t)]^T$ can be regarded as a mapping: $\mathrm{R}^{3N} \times S \times \mathrm{R} \mapsto \mathrm{R}^K$, where $S=\{s_1, \cdots, s_K\}$. $\boldsymbol{p}(\boldsymbol{r}, \boldsymbol{s};t)$ can be written as the product of the PDF $p(\boldsymbol{r}; t)$:$\mathrm{R}^{3N} \times \mathrm{R} \mapsto \mathrm{R}$ and the conditional PDF (cPDF) $\boldsymbol{p}(\boldsymbol{s}|\boldsymbol{r}; t) = [\boldsymbol{p}(s_1|\boldsymbol{r}; t), \cdots, \boldsymbol{p}(s_K|\boldsymbol{r}; t)]^T$:$S \times \mathrm{R} \mapsto [0, 1]^K$; that is, $\boldsymbol{p}(\boldsymbol{r}, \boldsymbol{s};t)=p(\boldsymbol{r};t)\boldsymbol{p}(\boldsymbol{s}|\boldsymbol{r};t)$. Differentiating it with respect to time yields

$$\frac{\partial \boldsymbol{p}(\boldsymbol{r}, \boldsymbol{s}; t)}{\partial t} = \frac{\partial p(\boldsymbol{r}; t)}{\partial t}\boldsymbol{p}(\boldsymbol{s}|\boldsymbol{r}; t) + \frac{\partial \boldsymbol{p}(\boldsymbol{s}|\boldsymbol{r}; t)}{\partial t}p(\boldsymbol{r}; t). \tag{6}$$

Consider that $\boldsymbol{r} \in \Omega \subset \mathbb{R}^{3N}$ is a "fast" variable for a continuous trajectory, where Ω is a connected and bounded domain. Then, $\partial p(\boldsymbol{r};t)/\partial t$ in Equation 6 can be formally written as $\partial p(\boldsymbol{r}; t)/\partial t = -\nabla_{\boldsymbol{r}} \cdot \boldsymbol{J}(\boldsymbol{r}, \boldsymbol{s}; t)$, where $\nabla_{\boldsymbol{r}}$ is the gradient operator, $\boldsymbol{J}(\boldsymbol{r}, \boldsymbol{s};t)=\boldsymbol{F}(\boldsymbol{r}, \boldsymbol{s};t)p(\boldsymbol{r};t)$ is the probability flux, and $\boldsymbol{F}(\boldsymbol{r}, \boldsymbol{s};t)$ is a velocity field. If we only consider isotropic diffusion and friction, then $\boldsymbol{F}(\boldsymbol{r}, \boldsymbol{s};t)$ can take the generalized Fokker–Planck approximation $\boldsymbol{F}(\boldsymbol{r}, \boldsymbol{s}; t) = \boldsymbol{V}(\boldsymbol{r}, \boldsymbol{s}; t) - \nabla_{\boldsymbol{r}}(D \log p(\boldsymbol{r}; t))$, where D is a diffusion coefficient. If we assume that changes in gene state do not contribute to chromatin motion, the velocity field $\boldsymbol{V}(\boldsymbol{r}, \boldsymbol{s};t)$ can be approximated by $\boldsymbol{V}(\boldsymbol{r};t)$. Then,

$$\frac{\partial p(\boldsymbol{r}; t)}{\partial t} = -\nabla_{\boldsymbol{r}} \cdot (\boldsymbol{V}(\boldsymbol{r}; t)p(\boldsymbol{r}; t)) + \nabla^2_{\boldsymbol{r}}(Dp(\boldsymbol{r}; t)), \tag{7}$$

where the first term represents the deterministic part, and the second term is a stochastic ingredient of the velocity field.

On the other hand, consider that gene state $\boldsymbol{s}$ is a "slow" variable in a discrete pathway. Then, $\partial \boldsymbol{p}(\boldsymbol{s}|\boldsymbol{r};t)/\partial t$ features the process of gene-state switching and can be written by a master equation:

$$\frac{\partial \boldsymbol{p}(\boldsymbol{s}|\boldsymbol{r}; t)}{\partial t} = \boldsymbol{W}(\boldsymbol{r}; t)\boldsymbol{p}(\boldsymbol{s}|\boldsymbol{r}; t), \tag{8}$$

where $\boldsymbol{W}(\boldsymbol{r};t)=(\lambda_{ij}(\boldsymbol{r};t))_{K\times K}$ is a nucleosome position–dependent state transition matrix, satisfying the conservative condition $\sum_{i=1}^{K} \lambda_{ij}(\boldsymbol{r}; t) = 0$.

We assume that tiny changes in nucleosome coordinates do not alter gene state, implying that the derivative of conditional probability, $\nabla_{\boldsymbol{r}}\boldsymbol{p}(\boldsymbol{s}|\boldsymbol{r};t)$, approximately equals zero partly because the time interval of downstream gene-state transition is generally longer than that of upstream chromatin motion (Lammers et al. 2020). Then, substituting Equations 7 and 8 into Equation 6 and using the assumption, we can obtain Equation 1.

Because we are interested in the effect of E-P communication on transcriptional bursting when the system is at a steady state (or after a long time), the initial conditions of Equation 1 become not so important. Meanwhile, because the chromatin chain is moving stochastically in a restricted nucleus space, reflecting boundaries of Equation 1 exist theoretically. However, because our model only focuses on the local structural dynamics of a segment of chromatin, we do not need to consider the behaviors of local motifs at the nuclear membrane boundary and assume that the boundary condition is a free boundary.

Simulation algorithm of 4D nucleome equation

Because of the coupling of the E-P communication and gene expression, we propose an algorithm to simulate the time evolution of the entire system.

Assume that there are L reactions involved in the gene-state switching process. The lth reaction propensity is denoted by $a_l(\boldsymbol{r},\boldsymbol{s};t)$, $l=1,2,\cdots,L$, and the total reaction propensity is calculated according to $a_{\text{tot}}(\boldsymbol{r},\boldsymbol{s};t)=\sum_{l=1}^{L}a_l(\boldsymbol{r},\boldsymbol{s};t)$. Note that $\boldsymbol{s}$ is the vector of all gene states, but in the following algorithm, we set the K−dimensional state vector $\boldsymbol{s}=\left[0,\cdots,0,\underset{j-\text{th}}{1},0,\cdots,0\right]^{\text{T}}$ when the current state is j in numerical simulation. Element v_{ij} of stoichiometric matrix $(v_{ij})_{K\times L}$ denotes the net change in gene state j owing to each reaction i, and $\boldsymbol{v}_\mu$ is the μth column of (v_{ij}). Let $H(\boldsymbol{r},\boldsymbol{s};t)$ be the survival probability that chromatin position is $\boldsymbol{r}$ and gene state is $\boldsymbol{s}$ state at time t. The main steps for solving Equation 1 are listed below.

1. Set the initial state as $\boldsymbol{r}_0=\boldsymbol{r}(t_0)$, $\boldsymbol{s}_0=\boldsymbol{s}(t_0)$.
2. Generate two random variables u_1 and u_2 distributed uniformly in interval (0, 1).
3. Integrate the system of stochastic differential equations

$$\begin{cases}\mathrm{d}\boldsymbol{r}=\boldsymbol{V}(\boldsymbol{r};t)\mathrm{d}t+\sqrt{2\boldsymbol{D}}\mathrm{d}\boldsymbol{B}(t),\\ \mathrm{d}H(\boldsymbol{r},\boldsymbol{s};t)=-a_{\text{tot}}(\boldsymbol{r},\boldsymbol{s};t)H(\boldsymbol{r},\boldsymbol{s};t)\mathrm{d}t,\\ \boldsymbol{r}(t_i)=\boldsymbol{r}_i,\ H(t_i)=1,\end{cases}$$

   from time points t_i to $t_i+\tau_i$, and with the stopping condition $H(\boldsymbol{r}_i,\boldsymbol{s}_i;t_i+\tau_i)=u_1$.
4. Update time and position: $t_{i+1}=t_i+\tau_i$, $\boldsymbol{r}_{i+1}=\boldsymbol{r}(t_{i+1})$.
5. Choose μ such that

$$\sum_{l=1}^{\mu-1}a_l(\boldsymbol{r}_{i+1},\boldsymbol{s}_i;t_{i+1})<u_2a_{\text{tot}}(\boldsymbol{r}_{i+1},\boldsymbol{s}_i;t_{i+1})\le\sum_{l=1}^{\mu}a_l(\boldsymbol{r}_{i+1},\boldsymbol{s}_i;t_{i+1}).$$

6. Update promoter state: $\boldsymbol{s}_{i+1}=\boldsymbol{s}_i+\boldsymbol{v}_\mu$.
7. Reiterate the system from Step 2 with a new state until a given largest time $t_{\max}$ is reached.

By the above algorithm steps, we can generate sample trajectories of the system.

Details of transcription model

The downstream bursting system to be studied is described by a set of biochemical reactions on a slow timescale in contrast to the chromatin motion on a fast timescale.

$$\begin{aligned}&\text{Chromatin opening:} && S_{\text{off2}}\xrightarrow{\lambda_{\text{on2}}}S_{\text{off1}},\\ &\text{Chromatin closure:} && S_{\text{off1}}\xrightarrow{\lambda_{\text{off2}}}S_{\text{off2}},\\ &\text{Burst initiation:} && S_{\text{off1}}\xrightarrow{\lambda_{\text{on1}}}S_{\text{rec}},\\ &\text{Pol II recruitment:} && S_{\text{rec}}\xrightarrow{\lambda_{\text{rec}}}S_{\text{rel}},\\ &\text{Pol II pause release:} && S_{\text{rel}}\xrightarrow{\lambda_{\text{rel}}}S_{\text{rec}}+\text{mRNA},\\ &\text{Burst termination1:} && S_{\text{rec}}\xrightarrow{\lambda_{\text{off1}}^{\text{rec}}}S_{\text{off1}},\\ &\text{Burst termination2:} && S_{\text{rel}}\xrightarrow{\lambda_{\text{off1}}^{\text{rel}}}S_{\text{off1}}.\end{aligned}$$

The details and rationality of the model are shown in Supplemental Text A.

Many biological processes require the participation of E-P communication (or the enhancer) (Supplemental Table S1). For example, enhancers recruit the Mediator complex or histone acetyltransferase EP300 to help the Pol II on promoters initiate transcription (Haberle and Stark 2018). Enhancers promote the dissociation of NELF by recruiting COFs to affect Pol II pause-release on promoter proximity (Aoi et al. 2020). Therefore, we assume the state-switching rate vector $\boldsymbol{\lambda}$ (consisting of λ_c, $c\in\{\text{on1, rec, rel}\}$) depends nonlinearly on the E-P spatial distance d_S and assumes $\boldsymbol{\lambda}=\boldsymbol{H}(d_s)$. The variable λ_c depending on the E-P spatial distance is

$$\lambda_c(d_S)=\begin{cases}\lambda_{c,\max}, & d_S\le\varepsilon_T,\\ \lambda_{c,\min}+(\lambda_{c,\max}-\lambda_{c,\min})/\left[1+\left(\dfrac{d_S-\varepsilon_T}{\varepsilon_{1/2}-\varepsilon_T}\right)^h\right], & d_S>\varepsilon_T,\end{cases}\quad(9)$$

where $\lambda_{c,\min}$ and $\lambda_{c,\max}$ are the minimum (basic) and maximum reaction rates, $\varepsilon_{1/2}$ is the spatial distance when λ_c is equal to $(\lambda_{c,\max}-\lambda_{c,\min})/2$, h is a Hill coefficient that controls how steep the rate curve is, and ε_T is a distance threshold. Equation 9 can illustrate how the transition rates vary with E-P topologies, and further indicates that transcription is regulated at any time (for more details information, see Supplemental Text A). The λ_c can be described using other function based on specific biological issues.

Statistical analysis of the whole model

In the simulation, we examine a system consisting of $N=100$ monomers in simulations. For a given set of parameters, we simulate 10^3 gene copies, proceeding through 10^7 sec in time. Each simulation starts in the OFF state. Before taking samples from every simulation, we run 10^4 sec to ensure equilibration in chromatin conformation and gene expression. After that, snapshots of the system are taken every 100 sec.

Using the data obtained by simulation, we perform statistical analysis for the chromatin structure, especially for the E-P spatial distance. Specifically, we calculate the PDF of E-P spatial distance based on the produced time series data. According to the reaction time series, we calculate the probability mass function (PMF) of BS and the PDFs of the dwell-time in S_{OFF} and S_{ON} states and the CT (the time from S_{OFF} to S_{ON} and back to S_{OFF}). Furthermore, we calculate some statistical quantities such as mean burst size (MBS), mean dwell-time (MDT) in ON/OFF state, mean cycle time (MCT), and BF. Here, MBS is defined as the average number of mRNA molecules produced per burst, whereas BF as the average number of bursts occurred in a given time interval. In other words, BF is the reciprocal of the MCT.

Theoretical analysis of transcriptional bursting

We derive the expressions of $p_{BS}(m)$ and $p_{CT}(t)$. For convenience, we uniformly denote these two distributions as $p_X(x)$.

To quantify the timescale separation, we introduce a parameter ω, which is defined as the ratio between the propensities of the

reactions on fast and slow timescales:

$$\omega = \frac{\min \lambda_{c,\min}}{\max V(\boldsymbol{r})},$$

where $\lambda_{c,\min}$, $c \in \{\text{on1, rec, rel}\}$ are the gene-state switching rates in downstream transcription processes, and $V(\boldsymbol{r})$ is the velocity field between the enhancer and the promoter in the upstream and is given by $V(\boldsymbol{r}) = (k_{NN}/d_G + k_{EP})d_S\gamma^{-1}$. The E-P velocity field equals $V(\boldsymbol{r}) = K_{EP}d_S/\gamma$, where K_{EP} represents the total spring coefficient between the enhancer and the promoter. We choose the value of d_S when the cumulative density function (CDF) of $p_{DS}(d_S)$ reaches 0.99, implying that the d_S reaches the maximum. Supplemental Figure S3, A and B, shows the effect of different parameters to ω.

In the case that the fluctuations in d_S are much faster compared with the rate of transcription, the d_S fluctuations can be averaged out, and the corresponding joint distribution denoted by $p^{\text{Fast}}_{X,DS}(x, d_S)$, which accounts for fluctuations in d_S and their effect on fluctuations in burst, is given by $p^{\text{Fast}}_{X,DS}(x, d_S) = p_X(x; \langle \boldsymbol{\lambda} \rangle)p_{DS}(d_S)$, where $\langle \boldsymbol{\lambda} \rangle = \int_0^{+\infty} \boldsymbol{H}(d_S)p_{DS}(d_S)\mathrm{d}d_S$. In this case, the marginal PDF (or PMF) of random variable X takes the form (Supplemental Fig. S3C,D)

$$p^{\text{Fast}}_X(x) = p_{X|\langle DS \rangle}\left(x \middle| \int_0^{+\infty} \boldsymbol{H}(d_S)p_{DS}(d_S)\mathrm{d}d_S\right). \tag{10}$$

Conversely, if fluctuations in d_S are much slower, the corresponding joint distribution denoted by $p^{\text{Slow}}_{X,DS}(x, d_S)$ is given by $p^{\text{Slow}}_{X,DS}(x, d_S) = p_{X|DS}(x|\boldsymbol{H}(d_S))p_{DS}(d_S)$. In this situation, the marginal PDF (or PMF) of random variable X takes the form (Supplemental Fig. S3E,F)

$$p^{\text{Slow}}_X(x) = \int_0^{+\infty} p_{X|DS}(x|\boldsymbol{H}(d_S))p_{DS}(d_S)\mathrm{d}d_S. \tag{11}$$

In general, the marginal PDF (or PMF) of X is a mixing distribution obtained by weighting the marginal PDF (or PMF); that is,

$$p_X(x) = \frac{1}{1+\omega}p^{\text{Fast}}_X(x) + \frac{\omega}{1+\omega}p^{\text{Slow}}_X(x). \tag{12}$$

The expectation of X can be expressed as

$$\langle X \rangle = \frac{1}{1+\omega}\langle X \rangle^{\text{Fast}} + \frac{\omega}{1+\omega}\langle X \rangle^{\text{Slow}}. \tag{13}$$

The detailed derivation process of the E-P spatial distance distribution $p_{DS}(d_S)$ is shown in Supplemental Text B. The downstream transcriptional bursting distribution (ignoring upstream E-P regulatory) can be obtained theoretically (for a more detailed derivation process, see Supplemental Text B).

Power laws for transcriptional bursting kinetics

The power h of the Hill function brings difficulties to the theoretical calculations of MBS and MCT. For this reason, we may use a deterministic binary rate for transcriptional burst for approximation and get the approximation expression of MBS_a and MCT_a (for more detailed expression, see Supplemental Text C).

To show the effects of increasing k_{EP} or d_G on MBS and BF, we calculate the following derivatives: $\partial\log_{10}\text{MBS}/\partial\log_{10}k_{EP}$ and $\partial\log_{10}\text{BF}/\partial\log_{10}k_{EP}$, $\partial\log_{10}\text{MBS}/\partial\log_{10}d_G$ and $\partial\log_{10}\text{BF}/\partial\log_{10}d_G$. We take the $\partial\log_{10}\text{MBS}/\partial\log_{10}k_{EP}$ as an example (for the explicit expression, see Supplemental Text C).

Through theoretical analysis and numerical calculation, we find $\partial\log_{10}\text{MBS}/\partial\log_{10}k_{EP}$ are positive when the parameters are not extreme (Supplemental Fig. S5A–C). They increase for small k_{EP} and then quickly decrease to zero with increasing k_{EP}. Meanwhile, the value of the derivatives changes little (the maximum values are not more than 0.8), implying that linear approximation is appropriate for $\log_{10}\text{MBS}(\log_{10}k_{EP})$ within an appropriate range of k_{EP}.

Assume that we can obtain $F(k_{EP_1}) \approx 1$ when k_{EP_1} is greater than a pregiven value, where F is the cumulative distribution of E-P spatial distance distribution, and $\lim_{k_{EP_2}\to 0} F(k_{EP_2}) \approx 0.0224$ where $d_G = 50$. We define

$$S_{BS} = \frac{\log_{10}\text{MBS}(k_{EP_1}) - \log_{10}\text{MBS}(k_{EP_2})}{\log_{10}k_{EP_1} - \log_{10}k_{EP_2}},$$

which represents the slope of the line of $\log_{10}\text{MBS}$ versus $\log_{10}k_{EP}$. Then, we obtain the following an approximate linear relation:

$$\begin{aligned}\log_{10}\text{MBS}(k_{EP}) &\approx S_{BS}\cdot(\log_{10}k_{EP} - \log_{10}k_{EP_1}) + \log_{10}(\text{BS}_{\max}) \\ &= S_{BS}\cdot\log_{10}k_{EP} + \log_{10}(\text{BS}_{\max}),\end{aligned}$$

which implies that MBS obeys the power law (Supplemental Fig. S6)

$$\text{MBS} \sim (k_{EP})^{S_{BS}}. \tag{14}$$

For the derivation process of other situations, see Supplemental Text C.

Software availability

The theoretical analysis and numerical simulation codes are provided as Supplemental Code and are available online at GitHub (https://github.com/cellfate/4DNucleome).

Competing interest statement

The authors declare no competing interests.

Acknowledgments

This work was supported by National Key R&D Program of China grant 2021YFA1302500; by Natural Science Foundation of P.R. China grants 12171494, 11931019, 11775314, 62373384, and 12301646; by Key-Area Research and Development Program of Guangzhou, P.R. China, grants 202007030004 and 2019B11 0233002; by Guangdong Basic and Applied Basic Research Foundation grants 2022A1515011540 and 2023A1515011982; by Guangdong Province Key Laboratory of Computational Science at the Sun Yat-sen University grant 2020B1212060032; by the Fundamental Research Funds for the Central Universities, Sun Yat-sen University grants 23qnpy48 and 23pnqy49; and by China Postdoctoral Science Foundation grant 2023M734061.

Author contributions: J.Z. conceived of the study. Z.W., Z.Z., S.L., and J.Z. implemented the method, performed the analysis, and interpreted the results. J.Z. supervised the study. Z.W., J.Z., and T.Z. drafted the manuscript with input from all the authors. All authors read and approved the final manuscript.

References

Alexander JM, Guan J, Li B, Maliskova L, Song M, Shen Y, Huang B, Lomvardas S, Weiner OD. 2019. Live-cell imaging reveals enhancer-dependent Sox2 transcription in the absence of enhancer proximity. *eLife* **8:** e41769. doi:10.7554/eLife.41769

Aoi Y, Smith ER, Shah AP, Rendleman EJ, Marshall SA, Woodfin AR, Chen FX, Shiekhattar R, Shilatifard A. 2020. NELF regulates a promoter-proximal step distinct from RNA Pol II pause-release. *Mol Cell* **78:** 261–274.e5. doi:10.1016/j.molcel.2020.02.014

Bartman CR, Hsu SC, Hsiung CC-S, Raj A, Blobel GA. 2016. Enhancer regulation of transcriptional bursting parameters revealed by forced chromatin looping. *Mol Cell* **62:** 237–247. doi:10.1016/j.molcel.2016.03.007

Bartman CR, Hamagami N, Keller CA, Giardine B, Hardison RC, Blobel GA, Raj A. 2019. Transcriptional burst initiation and polymerase pause release are key control points of transcriptional regulation. *Mol Cell* **73:** 519–532.e4. doi:10.1016/j.molcel.2018.11.004

Benabdallah NS, Williamson I, Illingworth RS, Kane L, Boyle S, Sengupta D, Grimes GR, Therizols P, Bickmore WA. 2019. Decreased enhancer-promoter proximity accompanying enhancer activation. *Mol Cell* **76:** 473–484.e7. doi:10.1016/j.molcel.2019.07.038

Bohrer CH, Larson DR. 2021. The stochastic genome and its role in gene expression. *Cold Spring Harb Perspect Biol* **13:** a040386. doi:10.1101/cshperspect.a040386

Bothma JP, Garcia HG, Ng S, Perry MW, Gregor T, Levine M. 2015. Enhancer additivity and non-additivity are determined by enhancer strength in the *Drosophila* embryo. *eLife* **4:** e07956. doi:10.7554/eLife.07956

Braichenko S, Holehouse J, Grima R. 2021. Distinguishing between models of mammalian gene expression: telegraph-like models versus mechanistic models. *J R Soc Interface* **18:** 20210510. doi:10.1098/rsif.2021.0510

Brivanlou AH, Darnell JE Jr. 2002. Signal transduction and the control of gene expression. *Science* **295:** 813–818. doi:10.1126/science.1066355

Brouwer I, Lenstra TL. 2019. Visualizing transcription: key to understanding gene expression dynamics. *Curr Opin Chem Biol* **51:** 122–129. doi:10.1016/j.cbpa.2019.05.031

Brueckner DB, Chen H, Barinov L, Zoller B, Gregor T. 2023. Stochastic motion and transcriptional dynamics of pairs of distal DNA loci on a compacted chromosome. *Science* **380:** 1357–1362. doi:10.1126/science.adf5568

Busslinger GA, Stocsits RR, Van Der Lelij P, Axelsson E, Tedeschi A, Galjart N, Peters J-M. 2017. Cohesin is positioned in mammalian genomes by transcription, CTCF and Wapl. *Nature* **544:** 503–507. doi:10.1038/nature22063

Cao Z, Filatova T, Oyarzún DA, Grima R. 2020. A stochastic model of gene expression with polymerase recruitment and pause release. *Biophys J* **119:** 1002–1014. doi:10.1016/j.bpj.2020.07.020

Cattoni DI, Gizzi AMC, Georgieva M, Di Stefano M, Valeri A, Chamousset D, Houbron C, Déjardin S, Fiche J-B, González I, et al. 2017. Single-cell absolute contact probability detection reveals chromosomes are organized by multiple low-frequency yet specific interactions. *Nat Commun* **8:** 1753. doi:10.1038/s41467-017-01962-x

Chen FX, Xie P, Collings CK, Cao K, Aoi Y, Marshall SA, Rendleman EJ, Ugarenko M, Ozark PA, Zhang A, et al. 2017. PAF1 regulation of promoter-proximal pause release via enhancer activation. *Science* **357:** 1294–1298. doi:10.1126/science.aan3269

Chen H, Levo M, Barinov L, Fujioka M, Jaynes JB, Gregor T. 2018. Dynamic interplay between enhancer–promoter topology and gene activity. *Nat Genet* **50:** 1296–1303. doi:10.1038/s41588-018-0175-z

Corrigan AM, Tunnacliffe E, Cannon D, Chubb JR. 2016. A continuum model of transcriptional bursting. *eLife* **5:** e13051. doi:10.7554/eLife.13051

Cover TM. 1999. *Elements of information theory*. John Wiley & Sons, Hoboken, NJ.

Dekker J, Mirny L. 2016. The 3D genome as moderator of chromosomal communication. *Cell* **164:** 1110–1121. doi:10.1016/j.cell.2016.02.007

Dekker J, Belmont A, Guttman M, Leshyk V, Lis J, Lomvardas S, Mirny L, O'Shea C, Park P, Ren B, et al. 2017. The 4D nucleome project. *Nature* **549:** 219–226. doi:10.1038/nature23884

Doi M, Edwards SF, Edwards S. 1988. *The theory of polymer dynamics*. Oxford University Press, New York.

Douglas AE. 2018. The *Drosophila* model for microbiome research. *Lab Anim (NY)* **47:** 157–164. doi:10.1038/s41684-018-0065-0

Fritzsch C, Baumgärtner S, Kuban M, Steinshorn D, Reid G, Legewie S. 2018. Estrogen-dependent control and cell-to-cell variability of transcriptional bursting. *Mol Syst Biol* **14:** e7678. doi:10.15252/msb.20177678

Fuda NJ, Ardehali MB, Lis JT. 2009. Defining mechanisms that regulate RNA polymerase II transcription in vivo. *Nature* **461:** 186–192. doi:10.1038/nature08449

Fukaya T, Lim B, Levine M. 2016. Enhancer control of transcriptional bursting. *Cell* **166:** 358–368. doi:10.1016/j.cell.2016.05.025

Gardiner CW. 2004. *Handbook of stochastic methods for physics, chemistry and the natural sciences*. Springer, Berlin Heidelberg.

Gizzi AMC, Cattoni DI, Fiche J-B, Espinola SM, Gurgo J, Messina O, Houbron C, Ogiyama Y, Papadopoulos GL, Cavalli G, et al. 2019. Microscopy-based chromosome conformation capture enables simultaneous visualization of genome organization and transcription in intact organisms. *Mol Cell* **74:** 212–222.e5. doi:10.1016/j.molcel.2019.01.011

Goutelle S, Maurin M, Rougier F, Barbaut X, Bourguignon L, Ducher M, Maire P. 2008. The Hill equation: a review of its capabilities in pharmacological modelling. *Fundam Clin Pharmacol* **22:** 633–648. doi:10.1111/j.1472-8206.2008.00633.x

Haberle V, Stark A. 2018. Eukaryotic core promoters and the functional basis of transcription initiation. *Nat Rev Mol Cell Biol* **19:** 621–637. doi:10.1038/s41580-018-0028-8

Harper CV, Finkenstädt B, Woodcock DJ, Friedrichsen S, Semprini S, Ashall L, Spiller DG, Mullins JJ, Rand DA, Davis JR, et al. 2011. Dynamic analysis of stochastic transcription cycles. *PLoS Biol* **9:** e1000607. doi:10.1371/journal.pbio.1000607

He B, Chen C, Teng L, Tan K. 2014. Global view of enhancer–promoter interactome in human cells. *Proc Natl Acad Sci* **111:** E2191–E2199.

Heinz S, Texari L, Hayes MG, Urbanowski M, Chang MW, Givarkes N, Rialdi A, White KM, Albrecht RA, Pache L, et al. 2018. Transcription elongation can affect genome 3D structure. *Cell* **174:** 1522–1536.e22. doi:10.1016/j.cell.2018.07.047

Heist T, Fukaya T, Levine M. 2019. Large distances separate coregulated genes in living *Drosophila* embryos. *Proc Natl Acad Sci* **116:** 15062–15067. doi:10.1073/pnas.1908962116

Henriques T, Scruggs BS, Inouye MO, Muse GW, Williams LH, Burkholder AB, Lavender CA, Fargo DC, Adelman K. 2018. Widespread transcriptional pausing and elongation control at enhancers. *Genes Dev* **32:** 26–41. doi:10.1101/gad.309351.117

Hübner MR, Eckersley-Maslin MA, Spector DL. 2013. Chromatin organization and transcriptional regulation. *Curr Opin Genet Dev* **23:** 89–95. doi:10.1016/j.gde.2012.11.006

Jennings BH. 2011. *Drosophila*: a versatile model in biology and medicine. *Mater Today* **14:** 190–195. doi:10.1016/S1369-7021(11)70113-4

Johnson DG, Walker CL. 1999. Cyclins and cell cycle checkpoints. *Annu Rev Pharmacol Toxicol* **39:** 295–312. doi:10.1146/annurev.pharmtox.39.1.295

Johnstone CP, Wang NB, Sevier SA, Galloway KE. 2020. Understanding and engineering chromatin as a dynamical system across length and timescales. *Cell Syst* **11:** 424–448. doi:10.1016/j.cels.2020.09.011

Jones DL, Brewster RC, Phillips R. 2014. Promoter architecture dictates cell-to-cell variability in gene expression. *Science* **346:** 1533–1536. doi:10.1126/science.1255301

Kan Z, States D, Gish W. 2002. Selecting for functional alternative splices in ESTs. *Genome Res* **12:** 1837–1845. doi:10.1101/gr.764102

Kandhavelu M, Häkkinen A, Yli-Harja O, Ribeiro AS. 2012. Single-molecule dynamics of transcription of the lar promoter. *Phys Biol* **9:** 026004. doi:10.1088/1478-3975/9/2/026004

Karmakar R. 2020. Control of noise in gene expression by transcriptional reinitiation. *J. Stat Mech Theory Exp* **2020:** 063402. doi:10.1088/1742-5468/ab8382

Karmakar R, Das AK. 2021. Effect of transcription reinitiation in stochastic gene expression. *J. Stat Mech Theory Exp* **2021:** 033502. doi:10.1088/1742-5468/abdeb1

Krebs AR, Imanci D, Hoerner L, Gaidatzis D, Burger L, Schübeler D. 2017. Genome-wide single-molecule footprinting reveals high RNA polymerase II turnover at paused promoters. *Mol Cell* **67:** 411–422.e4. doi:10.1016/j.molcel.2017.06.027

Kumar N, Platini T, Kulkarni RV. 2014. Exact distributions for stochastic gene expression models with bursting and feedback. *Phys Rev Lett* **113:** 268105. doi:10.1103/PhysRevLett.113.268105

Lammers NC, Kim YJ, Zhao J, Garcia HG. 2020. A matter of time: using dynamics and theory to uncover mechanisms of transcriptional bursting. *Curr Opin Cell Biol* **67:** 147–157. doi:10.1016/j.ceb.2020.08.001

Larson DR, Fritzsch C, Sun L, Meng X, Lawrence DS, Singer RH. 2013. Direct observation of frequency modulated transcription in single cells using light activation. *eLife* **2:** e00750. doi:10.7554/eLife.00750

Larsson AJM, Coucoravas C, Sandberg R, Reinius B. 2019a. X-Chromosome upregulation is driven by increased burst frequency. *Nat Struct Mol Biol* **26:** 963–969. doi:10.1038/s41594-019-0306-y

Larsson AJM, Johnsson P, Hagemann-Jensen M, Hartmanis L, Faridani OR, Reinius B, Segerstolpe Å, Rivera CM, Ren B, Sandberg R. 2019b. Genomic encoding of transcriptional burst kinetics. *Nature* **565:** 251–254. doi:10.1038/s41586-018-0836-1

Li J, Hsu A, Hua Y, Wang G, Cheng L, Ochiai H, Yamamoto T, Pertsinidis A. 2020. Single-gene imaging links genome topology, promoter–enhancer communication and transcription control. *Nat Struct Mol Biol* **27:** 1032–1040. doi:10.1038/s41594-020-0493-6

Li L, Waymack R, Gad M, Wunderlich Z. 2021. Two promoters integrate multiple enhancer inputs to drive wild-type knirps expression in the *Drosophila melanogaster* embryo. *Genetics* **219:** iyab154. doi:10.1093/genetics/iyab154

Lim B, Levine MS. 2021. Enhancer-promoter communication: hubs or loops? *Curr Opin Genet Dev* **67:** 5–9. doi:10.1016/j.gde.2020.10.001

Lim B, Heist T, Levine M, Fukaya T. 2018. Visualization of transvection in living *Drosophila* embryos. *Mol Cell* **70:** 287–296.e6. doi:10.1016/j.molcel.2018.02.029

Lu L, Liu X, Huang W-K, Giusti-Rodríguez P, Cui J, Zhang S, Xu W, Wen Z, Ma S, Rosen JD, et al. 2020. Robust Hi-C maps of enhancer-promoter interactions reveal the function of non-coding genome in neural development and diseases. *Mol Cell* **79:** 521–534.e15. doi:10.1016/j.molcel.2020.06.007

Marti-Renom MA, Almouzni G, Bickmore WA, Bystricky K, Cavalli G, Fraser P, Gasser SM, Giorgetti L, Heard E, Nicodemi M, et al. 2018. Challenges and guidelines toward 4D nucleome data and model standards. *Nat Genet* **50:** 1352–1358. doi:10.1038/s41588-018-0236-3

Misteli T. 2020. The self-organizing genome: principles of genome architecture and function. *Cell* **183:** 28–45. doi:10.1016/j.cell.2020.09.014

Murata M, Gong P, Suzuki K, Koizumi S. 1999. Differential metal response and regulation of human heavy metal-inducible genes. *J Cell Physiol* **180:** 105–113. doi:10.1002/(SICI)1097-4652(199907)180:1<105::AID-JCP12>3.0.CO;2-5

Neuert G, Munsky B, Rui ZT, Teytelman L, Khammash M, Oudenaarden AV. 2013. Systematic identification of signal-activated stochastic gene regulation. *Science* **339:** 584–587. doi:10.1126/science.1231456

Ochiai H, Hayashi T, Umeda M, Yoshimura M, Harada A, Shimizu Y, Nakano K, Saitoh N, Liu Z, Yamamoto T, et al. 2020. Genome-wide kinetic properties of transcriptional bursting in mouse embryonic stem cells. *Sci Adv* **6:** eaaz6699. doi:10.1126/sciadv.aaz6699

Ou HD, Phan S, Deerinck TJ, Thor A, Ellisman MH, O'shea CC. 2017. ChromEMT: visualizing 3D chromatin structure and compaction in interphase and mitotic cells. *Science* **357:** eaag0025. doi:10.1126/science.aag0025

Perry MW, Boettiger AN, Bothma JP, Levine M. 2010. Shadow enhancers foster robustness of *Drosophila* gastrulation. *Curr Biol* **20:** 1562–1567. doi:10.1016/j.cub.2010.07.043

Pott S, Lieb JD. 2015. What are super-enhancers? *Nat Genet* **47:** 8–12. doi:10.1038/ng.3167

Robson MI, Ringel AR, Mundlos S. 2019. Regulatory landscaping: how enhancer-promoter communication is sculpted in 3D. *Mol Cell* **74:** 1110–1122. doi:10.1016/j.molcel.2019.05.032

Rodriguez J, Larson DR. 2020. Transcription in living cells: molecular mechanisms of bursting. *Annu Rev Biochem* **89:** 189–212. doi:10.1146/annurev-biochem-011520-105250

Rodriguez J, Ren G, Day CR, Zhao K, Chow CC, Larson DR. 2019. Intrinsic dynamics of a human gene reveal the basis of expression heterogeneity. *Cell* **176:** 213–226.e18. doi:10.1016/j.cell.2018.11.026

Senecal A, Munsky B, Proux F, Ly N, Braye FE, Zimmer C, Mueller F, Darzacq X. 2014. Transcription factors modulate c-Fos transcriptional bursts. *Cell Rep* **8:** 75–83. doi:10.1016/j.celrep.2014.05.053

Shahrezaei V, Swain PS. 2008. Analytical distributions for stochastic gene expression. *Proc Natl Acad Sci* **105:** 17256–17261. doi:10.1073/pnas.0803850105

Shannon CE. 1948. A mathematical theory of communication. *Bell Syst Tech J* **27:** 379–423. doi:10.1002/j.1538-7305.1948.tb01338.x

Shao W, Zeitlinger J. 2017. Paused RNA polymerase II inhibits new transcriptional initiation. *Nat Genet* **49:** 1045–1051. doi:10.1038/ng.3867

Sood V, Misteli T. 2022. The stochastic nature of genome organization and function. *Curr Opin Genet Dev* **72:** 45–52. doi:10.1016/j.gde.2021.10.004

Stadhouders R, Filion GJ, Graf T. 2019. Transcription factors and 3D genome conformation in cell-fate decisions. *Nature* **569:** 345–354. doi:10.1038/s41586-019-1182-7

Stavreva DA, Coulon A, Baek S, Sung MH, John S, Stixova L, Tesikova M, Hakim O, Miranda T, Hawkins M, et al. 2015. Dynamics of chromatin accessibility and long-range interactions in response to glucocorticoid pulsing. *Genome Res* **25:** 845–857. doi:10.1101/gr.184168.114

Su J-H, Zheng P, Kinrot SS, Bintu B, Zhuang X. 2020. Genome-scale imaging of the 3D organization and transcriptional activity of chromatin. *Cell* **182:** 1641–1659.e26. doi:10.1016/j.cell.2020.07.032

Suter DM, Molina N, Gatfield D, Schneider K, Schibler U, Naef F. 2011. Mammalian genes are transcribed with widely different bursting kinetics. *Science* **332:** 472–474. doi:10.1126/science.1198817

Sutherland HG, Martin DI, Whitelaw E. 1997. A globin enhancer acts by increasing the proportion of erythrocytes expressing a linked transgene. *Mol Cell Biol* **17:** 1607–1614. doi:10.1128/MCB.17.3.1607

Szavits-Nossan J, Grima R. 2023. Steady-state distributions of nascent RNA for general initiation mechanisms. *Phys Rev Res* **5:** 013064. doi:10.1103/PhysRevResearch.5.013064

Thomas P, Popović N, Grima R. 2014. Phenotypic switching in gene regulatory networks. *Proc Natl Acad Sci* **111:** 6994–6999. doi:10.1073/pnas.1400049111

Tunnacliffe E, Chubb JR. 2020. What is a transcriptional burst? *Trends Genet* **36:** 288–297. doi:10.1016/j.tig.2020.01.003

Walters MC, Fiering S, Eidemiller J, Magis W, Groudine M, Martin D. 1995. Enhancers increase the probability but not the level of gene expression. *Proc Natl Acad Sci* **92:** 7125–7129. doi:10.1073/pnas.92.15.7125

Wang Z, Zhang Z, Zhou T. 2020. Exact distributions for stochastic models of gene expression with arbitrary regulation. *Sci China Math* **63:** 485–500. doi:10.1007/s11425-019-1622-8

Weidemann DE, Holehouse J, Singh A, Grima R, Hauf S. 2023. The minimal intrinsic stochasticity of constitutively expressed eukaryotic genes is sub-Poissonian. *Sci Adv* **9:** eadh5138. doi:10.1126/sciadv.adh5138

Xiao JY, Hafner A, Boettiger AN. 2021. How subtle changes in 3D structure can create large changes in transcription. *eLife* **10:** e64320. doi:10.7554/eLife.64320

Yokoshi M, Segawa K, Fukaya T. 2020. Visualizing the role of boundary elements in enhancer-promoter communication. *Mol Cell* **78:** 224–235.e5. doi:10.1016/j.molcel.2020.02.007

Zabidi MA, Stark A. 2016. Regulatory enhancer–core-promoter communication via transcription factors and cofactors. *Trends Genet* **32:** 801–814. doi:10.1016/j.tig.2016.10.003

Zhang J, Zhou T. 2014. Promoter-mediated transcriptional dynamics. *Biophys J* **106:** 479–488. doi:10.1016/j.bpj.2013.12.011

Zhang J, Zhou T. 2019. Markovian approaches to modeling intracellular reaction processes with molecular memory. *Proc Natl Acad Sci* **116:** 23542–23550. doi:10.1073/pnas.1913926116

Zuin J, Roth G, Zhan Y, Cramard J, Redolfi J, Piskadlo E, Mach P, Kryzhanovska M, Tihanyi G, Kohler H, et al. 2022. Nonlinear control of transcription through enhancer–promoter interactions. *Nature* **604:** 571–577. doi:10.1038/s41586-022-04570-y

Received April 12, 2023; accepted in revised form December 18, 2023.